Dynamical Patterns in Arrays of Coupled Chemical Oscillators and Excitators

V. Votrubová, P. Hasal,* L. Schreiberová, and M. Marek

Department of Chemical Engineering and Center for Nonlinear Dynamics of Chemical and Biological Systems, Faculty of Chemical Engineering, Institute of Chemical Technology, Prague, 166 28 Prague 6, Czech Republic

Received: September 17, 1997; In Final Form: December 1, 1997

Dynamical regimes arising due to mutual interactions of oscillatory and excitatory modes of the Belousov−Zhabotinskii (BZ) reaction in a two-array and linear and circular three-arrays (with different arrangements of intrinsic connections) of identical continuous stirred tank reactors (CSTRs) coupled via symmetric passive diffusion/convection mass exchange were studied both experimentally and by numerical simulations. The coupling strength among individual CSTRs and the threshold of excitability of the BZ reaction mixture were varied systematically. Firing numbers (vectors) were used for classification of observed oscillatory−excitatory modes. Full spectra of firing numbers ranging from 0 to 1 were detected in all CSTR arrays investigated in experiments. The numbers of oscillators and excitators, threshold of excitability, and the way of coupling and coupling strengths within the array are principal factors affecting firing patterns of the array. Numerical simulations with the dimensionless three-variable Oregonator based model of the BZ reaction predict qualitatively well dynamical regimes encountered in experiments. Noisy coupling among the individual CSTRs due to hydrodynamical fluctuations is suggested to explain some of the observed differences.

1. Introduction

Coupling of elementary dynamical units into structured networks represents standard way of construction of cognitive structures encountered mainly in living systems (e.g., neural networks). Oscillatory, excitable, or multistable units are basic elements of such networks. These elements can be modeled by chemical and biochemical reaction systems in continuous stirred tank reactors (CSTRs) interconnected by means of mass and/or information exchange. Experiments with such systems are usually performed under more strictly controlled experimental conditions than is possible with biological systems. The well-founded kinetic models can be used for interpretation of results observed in model chemical systems and conclusions resulting from such interpretation can yield generic features of the dynamics of these systems that are extendable to more complex biological systems.

Three ways of coupling of elementary units (CSTRs) are commonly used in chemical systems: (i) passive direct mutual mass-flow coupling, (ii) coupling via active pumping, and (iii) electric current or potential coupling. The passive mutual mass-flow coupling of chemical units takes usually the form of a convective and/or diffusional mass exchange through apertures (channels) in walls shared by adjacent units. The coupling is symmetric if volumes of the coupled units do not differ. The passive coupling is used very frequently in studies on coupled chemical oscillators or excitators.[1−13] The active pumping[14−19] enables asymmetric coupling even among the units of equal volumes and is usually performed by means of peristaltic pumps. Yoshimoto et al.[19] studied experimentally synchronizations of three circularly coupled Belousov−Zhabotinskii (BZ) oscillators in a system with active pumping. A wide variety of dynamical modes were observed under both symmetric and asymmetric coupling. Studies on pattern recognition by means of networks of coupled CSTRs with bistable chemical reaction (the iodate−arsenous acid reaction)[20−26] were performed, tuning the coupling strengths of individual pairs of units in the network in the course of the learning phase of the pattern recognition process. The electric current or potential coupling (also in combination with the controlled mass-flow coupling) was also used in the studies of dynamical regimes of the BZ reaction in coupled CSTRs.[27−30]

The information in complex biological systems is often encoded in sequences of firings of excitable elements of the networks. The evaluation of the received signals also occurs by synchronized firings of individual network elements (e.g., receptors in the retina or neurons in the cortex). The principles underlying the mechanism of response of coupled cells to pulsed or oscillatory stimulations and resulting firing patterns are therefore a subject of continuous interest. Considerable effort was devoted to both experimental and theoretical studies of coupled chemical excitators. Propagation of an excitable response to single and periodic pulsed perturbations in networks of coupled CSTRs was a main goal of these studies.[31−37] Marek and Schreiber[31] reviewed dynamical regimes arising in periodically stimulated coupled chemical excitators and on several examples demonstrated techniques used for analysis and classification of such regimes. Experimental studies of resonance regimes arising as a response to single or periodic stimulations by concentration pulses in arrays of coupled CSTRs with the BZ reaction have been the subject of several papers.[32−34] Numerical studies were also performed using various kinetic models.[35,36] Excitation diagrams representing dependence of excitatory modes on the period and the amplitude of perturbations were constructed and also one-dimensional maps called phase excitation curves were used for the description of the observed regimes. Both periodic and aperiodic excitatory regimes were observed together with the propagation failure phenomena (cessation of the propagation of excitable response from the perturbed CSTR to unperturbed ones) within defined range of experimental conditions.

* To whom correspondence should be addressed. e-mail: hasalp@tiger.vscht.cz.

S1089-5639(97)03041-7 CCC: $15.00
Published on Web 02/03/1998

Contrary to existence of extensive literature on arrays of coupled oscillators and on arrays of coupled excitators, very limited attention was devoted to study of dynamical behavior of the oscillatory and excitatory elements coupled mutually within one array where oscillators act as pacemakers perturbing the coupled excitators. Such arrays combining together oscillatory and excitatory subunits are more frequently encountered in biology and physiology (e.g., in the form of mutually coupled neurons). For example, Terman and Lee[38] studied a model network of neural oscillators and excitators with couplings modeled in a way mimicking chemical synapses. Kopell and Somers[39] analyzed stability of antiphase solutions in a system of two relaxation oscillators coupled through excitatory interactions. The literature on systems of coupled chemical oscillators and excitators in CSTRs is very scarce. Coupling of two BZ oscillators in CSTRs of different volumes connected via a tube filled with an excitable reaction−diffusion medium (a silica gel with immobilized ferroin) was reported by Stössel and Münster.[40] One of the oscillators (the larger one) forced the excitable medium in the tube transferring the perturbation to the second (the smaller one or target) oscillator. Both periodic entrainment and aperiodic regimes were observed depending on the residence times in both reactors. Propagation of oscillations from a CSTR with the BZ reaction into connected tubular (unstirred) reactor under oscillatory conditions was experimentally followed by Marek and Svobodová.[41]

In this paper we present results of an introductory study of mutual interactions among the BZ oscillators and excitators in linear two- and three-arrays and in circular three-arrays consisting of CSTRs coupled via passive mutual mass exchange. The results of experiments are compared to results of numerical simulations using a three component dimensionless model of the BZ reaction kinetics.

2. Experimental Section

All experiments were carried out in a system of three reaction cells (CSTRs) with direct mutual mass-exchange coupling described in detail in previous paper.[42] The intensity of mass-exchange coupling among the CSTRs is characterized by the value of mass transport coefficient k_d defined as the ratio of the volumetric flow rate between the adjacent cells to volume of the cell. The value of the coefficient k_d is adjustable within the interval $0-0.025\ s^{-1}$ by means of movable intercell barriers. The coupling between the cells was symmetric in all cell array configurations used in experiments due to equal volume of all cells in the array. The intensity of mass exchange was set to the same value for all pairs of adjacent cells in an array. Platinum electrodes were used to measure the redox potential E_{Pt} in all cells (the calomel electrode was used as the reference one and the potentials were registered by a computer after AD conversion). The temperature inside the cells was measured by a thermistor and controlled by a water bath circulator (see Nevoral et al.[42] for details).

The controlled stirring speed of the four-bladed Rushton-turbine type impellers was set to 350 min^{-1}. The mean residence time of reaction mixture in all cells was 30 min (the single cell volume is 30 cm^3) and reaction temperature was set to 28 ± 0.1 °C in all experiments. The reactant streams were preheated in water bath before entering the reactor. All chemicals used in the experiments were of reagent grade.

The reactants were delivered in three separate streams into each reaction cell. The inlet concentrations of reactants (related to cell volume) were

inlet stream 1: $[Ce(SO_4)_2]_0 = 0.006$ mol dm^{-3}

$[H_2SO_4]_0 = 0.410$ mol dm^{-3}

inlet stream 2: $[CH_2(COOH)_2]_0 = 0.100$ mol dm^{-3}

$[NaBrO_3]_0 = 0.200$ mol dm^{-3}

inlet stream 3: $[KBr]_0 = 0.000-0.010$ mol dm^{-3}

Various levels of inlet KBr concentration in the inlet stream 3 were used in order to change the threshold of excitability of reaction mixture in the excitatory cells. No KBr was fed to reaction cells with the BZ reaction set to the mode of autonomous oscillations. The period of autonomous oscillations under given experimental conditions was approximatelly 57.5 s and remained the same in all experiments. The reaction cell system can be operated either as a linear array of two or three cells or as a circular array of three cells. Possible configurations of oscillatory and excitatory cells within two- and three-arrays of reaction cells are displayed in Figure 1.

The values of the mass-transfer coefficient k_d and of the inlet KBr concentration (Br^- ions control the magnitude of the threshold of excitability of the BZ reaction mixture) have been varied systematically in experiments and the time traces of E_{Pt} in individual cells were recorded and stored for the subsequent evaluation of observed oscillatory−excitatory patterns.

3. Numerical Simulations

Dynamical behavior of coupled excitatory and oscillatory cell arrays was numerically simulated using the set of mass balance equations for key reaction components. The mass balances in dimensionless form are

$$\frac{d\xi_{ij}}{d\tau} = \varphi_{ij} + \kappa_0(\xi_{ij}^0 - \xi_{ij}) + \kappa_d(\xi_{i,j-1} - 2\xi_{ij} + \xi_{i,j+1}) \quad (1)$$

where ξ_{ij} represents dimensionless concentration of the ith component in the jth cell, ξ_{ij}^0 is its dimensionless inlet concentration, and τ is dimensionless time. Parameter κ_d expresses dimensionless coupling strength coefficient and κ_0 is dimensionless reciprocal residence time in the single cell. The index j ($j = 1$ and 2 for a two-array and $j = 1$, 2, and 3 for three-arrays) denotes position of the reaction cell within the array (cf Figure 1). Boundary conditions for the sets of eqs 1 are (i) $\xi_{i0} = \xi_{i1}$ and $\xi_{i3} = \xi_{i2}$ for two-array, and (ii) $\xi_{i0} = \xi_{i1}$ and $\xi_{i4} = \xi_{i3}$ for the linear three-array, (iii) $\xi_{i0} = \xi_{i3}$ and $\xi_{i4} = \xi_{i1}$ for the circular three-array, respectively. Here we adopt the three-variable Oregonator based model of the BZ reaction[43,44] (i.e., $i = 1$, 2, and 3). Dimensionless reaction rates φ_{ij} in eq 1 are given by the relations

$$\varphi_{1j} = \frac{1}{\epsilon}(x_j - \kappa_{-5}u_j^2 - x_jy_j + py_j - x_j^2) \quad (2)$$

$$\varphi_{2j} = \frac{1}{\epsilon\sigma}(qz_1 - py_1 - x_1y_1 + \kappa_9) \quad (3)$$

$$\varphi_{3j} = 2(x_1 - \kappa_{-5}u_1^2) - z_1 \quad (4)$$

Here $x_j \equiv \xi_{1j}$, $y_j \equiv \xi_{2j}$, and $z_j \equiv \xi_{3j}$ are dimensionless concentrations of reaction components $HBrO_2$, Br^-, and Ce^{4+} in the jth cell, respectively. The parameter q is stoichiometric factor of the BZ reaction.[43,44] The dimensionless concentrations

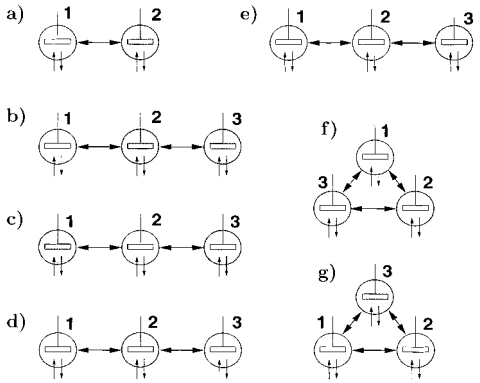

Figure 1. Arrays of coupled BZ oscillators (empty cells, **O**) and excitators (shadowed cells, **E**). (a) two-array **OE**. (b) linear three-array **OEE**. (c) linear three-array **EOE**. (d) linear three-array **OEO**. (e) linear three-array **OOE**. (f) circular three-array **cOEE**. (g) circular three-array **cOOE**.

of reaction components and other model parameters are defined in the Appendix.

4. Results and Discussion

Firing numbers of individual excitators within the array were used for the classification of particular oscillatory−excitatory dynamical patterns observed in experiments and numerical simulations. The firing number σ_{km} of the kth excitator with respect to the mth oscillator is defined as

$$\sigma_{km} = \frac{n_k^e}{n_m^o} \tag{5}$$

where n_k^e is the number of excitations observed in the kth cell over a (long) time interval Δt and n_m^o is the number of oscillations in the mth oscillatory cell completed over the same time interval Δt. The indexing of individual reaction cells within the investigated arrays is given in Figure 1. The full set of firing numbers σ_{km} for all excitators with respect to all oscillators in a general coupled cell array with M oscillators and K excitators form an *excitation matrix* $\sigma = (\sigma_{km}; k = 1, ... K; M \equiv 1, ..., M)$ which can be used for representation of the dynamic behavior of entire array.

Firing numbers σ_{km} are used for construction of either excitation diagrams (plots of firing numbers vs coupling strength coefficient at given inlet Br^- concentration) or phase excitation diagrams showing a partitioning of the parametric phase plane coupling strength coefficient versus inlet Br^- concentration (model variable Y_j^0) into regions corresponding to oscillatory−excitatory regimes characterized by particular values of firing numbers.

4.1. Experimental Results. *Two-array OE*. The most simple coupled cell array (i.e., the oscillator−excitator two-array (**OE**)) was studied first to map the distribution of dynamical regimes in the parametric space of chosen adjustable experimental parameters. Figure 2 shows evolution of signals from both cells of the **OE** array under increasing coupling strength and at constant value of the threshold of excitability of the BZ reaction mixture. Aperiodic (irregular) firings in the excitatory cell are observed at weak couplings, then the periodic regime with $\sigma_{21} = 0.5$ is established after small increase of the coupling strength, and finally, the full excitation regime with $\sigma_{21} = 1$ is reached when strong coupling is used.

Excitation diagrams (i.e., the dependences of the firing number σ_{21} on the coupling strength coefficient k_d at different

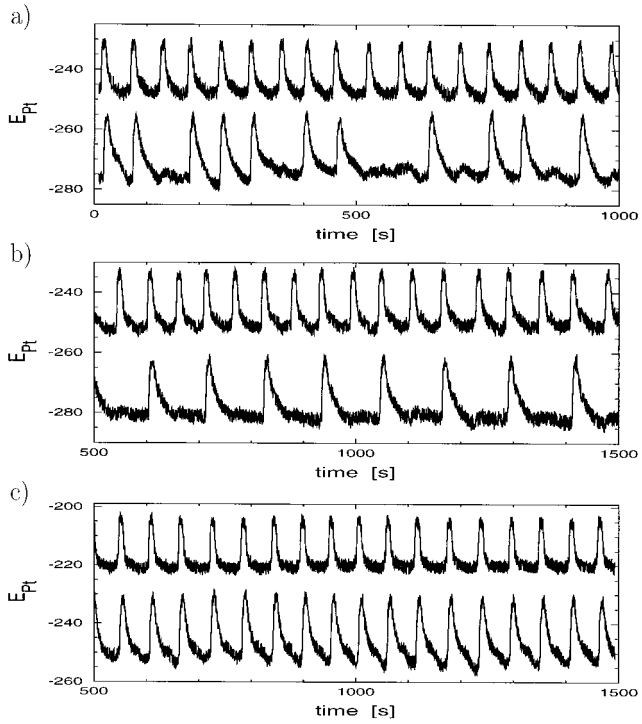

Figure 2. Experimental time traces of Pt electrode potentials from two-array **OE**. Inlet KBr concentration: $Y_2^0 = 0.004$ mol dm^{-3}; upper traces, oscillatory cell; lower traces, excitatory cell. Coupling strength coefficient values: (a) $k_d = 6.656 \times 10^{-3}$ s^{-1}, aperiodic regime with $\sigma_{21} < 1$. (b) $k_d = 6.937 \times 10^{-3}$ s^{-1}, periodic regime with $\sigma_{21} = 1/2$. (c) $k_d = 9.420 \times 10^{-3}$ s^{-1}, periodic regime with $\sigma_{21} = 1$.

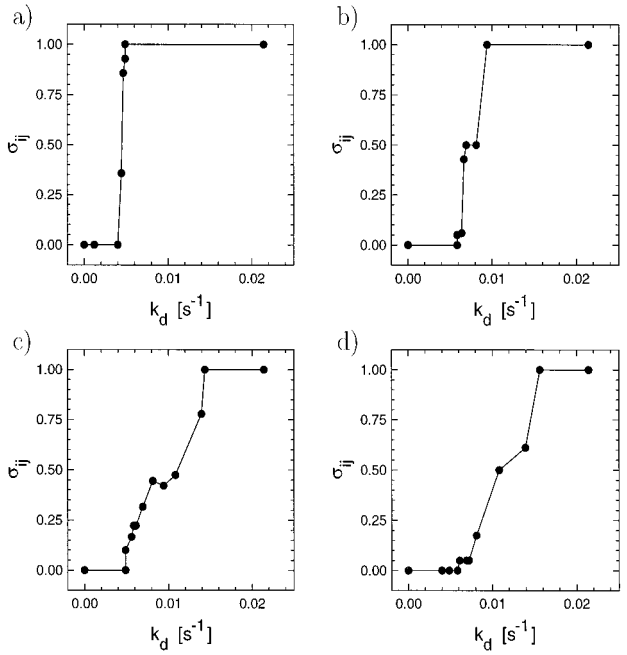

Figure 3. Experimental excitation diagrams for two-array **OE** ($i \equiv 2$, $j \equiv 1$). Inlet KBr concentration: (a) $Y_2^0 = 0.003$ mol dm^{-3}. (b) $Y_2^0 = 0.004$ mol dm^{-3}, (c) $Y_2^0 = 0.005$ mol dm^{-3}, (d) $Y_2^0 = 0.006$ mol dm^{-3}.

values of inlet KBr concentration) are depicted in Figure 3. No firings in the excitatory cell (no-excitation regime, $\sigma_{21} = 0$) occur below certain minimum coupling strength value which slightly increases with the increasing inlet KBr concentration (i.e., with the increasing excitability threshold). Steep transition from the no-excitation regime to the full excitation one ($\sigma_{21} = 1$) was observed at the lowest inlet KBr concentration (cf Figure

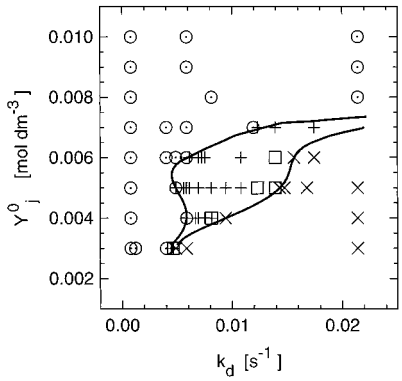

Figure 4. Experimental phase excitation diagram for two-array **OE** ($i \equiv 2, j \equiv 1$). ($\odot$) $\sigma_{21} = 0$. (+) $0 < \sigma_{21} < {}^1/_2$. ($\square$) ${}^1/_2 \leq \sigma_{21} < 1$. ($\times$) $\sigma_{21} = 1.0$

3a). At the inlet KBr concentration equal to 0.004 mol dm^{-3} a noticeable plateau of the firing number $\sigma_{21} = 0.5$ appears in the excitation diagram (cf Figure 3b). At further increased values of the inlet KBr concentration (0.005 and 0.006 mol dm^{-3}), the transitions from the no-excitation regime to the full excitation one are gradual and a number of fractional excitation regimes ($0 < \sigma_{21} < 1$) can be detected (cf Figure 3c,d). The global overview of the occurrence of excitatory−oscillatory regimes observed in experiments is given in the phase excitation diagram in Figure 4. Three regions are clearly visible in Figure 4: (i) the region of no excitations at low coupling strength and/or high inlet KBr concentration, (ii) the region of full excitation at high coupling strength and low inlet KBr concentration, and (iii) the region of fractional excitations located between previous two regions. Most of the oscillatory−excitatory regimes within this region belong to aperiodic ones. Two subregions of the fractional excitation region can be roughly identified: a region with $\sigma_{21} < 0.5$ and a region with $\sigma_{21} > 0.5$. The phase excitation diagram in Figure 4 indicates that the region of the fractional excitation regimes is relatively narrow (extending at most over one-third of the experimentally available coupling strength values). Precise tuning of the coupling strength among two interacting cells is therefore necessary in order to obtain an excitation regime with required value of firing number. No windows of the excitation failure (cf Kosek and Marek[45] and Nevoral et al.[42]) were observed within the region of full excitation as both the period and the amplitude of stimulation of the excitable cell by the oscillations in the oscillatory cell are sufficiently large. No excitations over the studied range of coupling strength values were detected at inlet KBr concentration higher or equal to approximately 0.007 mol dm^{-3}. The region of the excitation regimes accessible for experiments is bounded from below by the inlet KBr concentration equal approximately to 0.003 mol dm^{-3} as the BZ reaction mixture tends to exhibit spontaneous excitations and/or autonomous oscillations at lower values of the inlet KBr concentration.

Four distinct values of the inlet KBr concentration were chosen for experiments with coupled cell three-arrays: 0.003, 0.004, 0.005, and 0.006 mol dm^{-3}. The linear three-arrays **OEE** and **EOE** and the circular three-array **cOEE** were chosen for experiments.

*Linear Three-Array **OEE***. An example of a record of the almost periodic oscillatory−excitatory pattern from the linear three-array **OEE** with synchronized fractional firings in both excitators (i.e., $\sigma_{21} = \sigma_{31} \doteq 0.333$, is shown in Figure 5a. The excitation diagrams in Figure 6 elucidate deep changes in the excitatory dynamics of the linear **OEE** three-array compared to excitatory behavior of the **OE** array. No firings in the

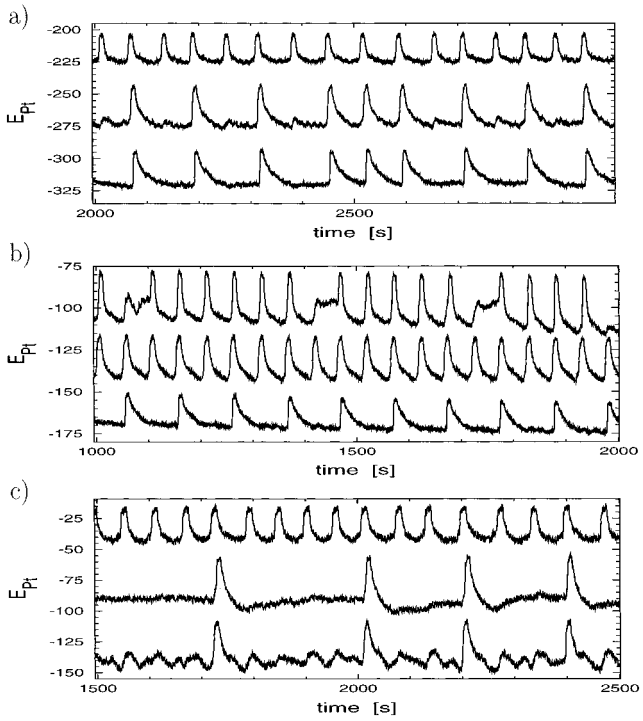

Figure 5. Experimental time traces of Pt electrode potentials in three-arrays of coupled cells. (a) linear array **OEE**, $k_d = 1.311 \times 10^{-2}$ s^{-1}; $Y_2^0 = Y_3^0 = 0.003$ mol dm^{-3}. Upper trace, cell 1—oscillatory; middle trace: cell 2—excitatory; lower trace, cell 3—excitatory. (b) linear array **EOE**; $k_d = 5.904 \times 10^{-3}$ s^{-1}; $Y_1^0 = Y_3^0 = 0.003$ mol dm^{-3}. Upper trace, cell 1—excitatory; middle trace, cell 2—oscillatory; lower trace, cell 3—excitatory. (c) circular array **cOEE**; $k_d = 2.026 \times 10^{-3}$ s^{-1}; $Y_2^0 = Y_3^0 = 0.004$ mol dm^{-3}. Upper trace, cell 1—oscillatory; middle trace, cell 2—excitatory; lower trace, cell 3—excitatory.

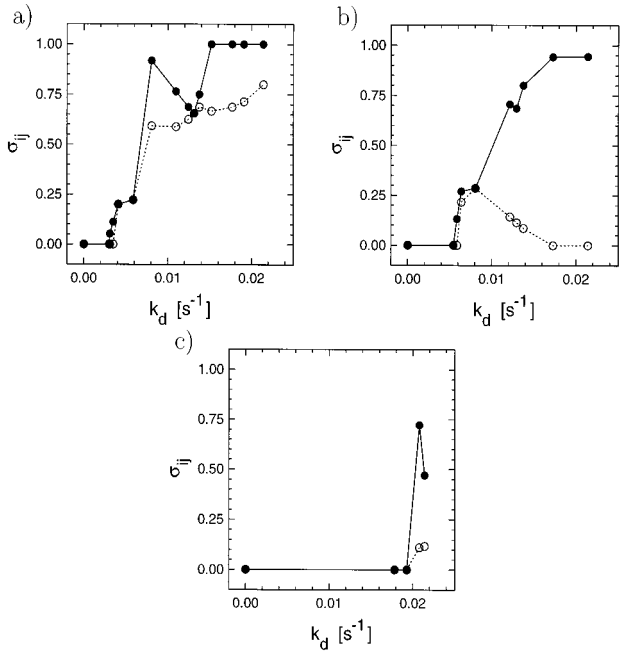

Figure 6. Experimental excitation diagrams for linear three-array OEE. (●) firing number σ_{21}. (○) Firing number σ_{31}. Inlet KBr concentration: (a) $Y_2^0 = Y_3^0 = 0.003$ mol dm^{-3}, (b) $Y_2^0 = Y_3^0 = 0.004$ mol dm^{-3}, (c) $Y_2^0 = Y_3^0 = 0.005$ mol dm^{-3}.

excitatory cells occur at values of coupling strengths below a threshold value which markedly increases with the increasing inlet KBr concentration. No excitations in both excitatory cells are possible above KBr concentration approximately equal to

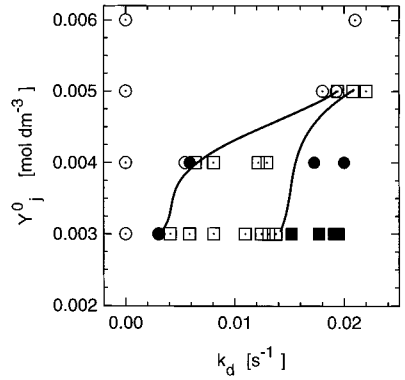

Figure 7. Experimental phase excitation diagram for linear three-array **OEE**, ($j \equiv 2, 3$). (⊙) $\sigma_{21} = \sigma_{31} = 0$. (●) $0 < \sigma_{21} < 1$, $\sigma_{31} = 0$. (⊡) $0 < (\sigma_{21}, \sigma_{31}) < 1$. (■) $\sigma_{21} = 1$, $0 < \sigma_{31} < 1$.

0.005 mol dm^{-3} as can be seen from the phase excitation diagram shown in Figure 7. The excitatory regimes observed in the linear **OEE** array belong mostly to unsynchronized ones, (i.e., $\sigma_{21} \neq \sigma_{31}$). Only the regimes with low firing numbers ($\sigma_{ij} \leq 0.25$) observed at weak coupling and the full excitation regimes are synchronized. These experimental observations differ markedly from excitatory regimes observed by Nevoral et al.[42] in the **EEE** array with pulsed perturbations where only synchronized firings in the second and the third cells were detected.

The excitations in the **OEE** array partly or completely fail to propagate from the first excitatory cell to the second one with the increasing inlet KBr concentration. The oscillatory perturbation from the oscillatory cell (which stimulates the neighboring cell continuously contrary to the pulsed perturbation) is being immediatelly diluted throughout entire volume in the course of its spreading to the perturbed cell, and moreover, it is at the same time further smeared out by partial transport of reaction components to the next coupled excitator. The amplitudes of perturbations delivered to both excitable cells therefore decrease and are thus uncapable to evoke firings, especially when the threshold of the excitability is high (high inlet KBr concentration). Figure 6a−c illustrate the transitions of the excitatory patterns from the no-excitation regime to the fractional excitation regimes occupying nearly entire range of experimentally accessible coupling strengths with the increasing KBr concentration. No substantial continuous subregions characterized by constant values of firing numbers σ_{21} and σ_{31} were found within the region of fractional firings. The extinction of excitations in the second excitator is also documented in excitation diagrams. A nonmonotonic increase in firing number values in the excitation diagrams in Figure 6 is due to imprecise experimental adjustments of the coupling strengths among the cells.

*Linear Three-Array **EOE***. Both excitatory cells in the linear array **EOE** are simultaneously perturbed due to their direct coupling to the oscillatory cell. The synchronized firings in both excitators are therefore likely to be observed. In experiments, however, the unsynchronized regimes ($\sigma_{12} \neq \sigma_{32}$) were frequently recorded. Figure 5b shows records of Pt electrode potentials from all cells at weak coupling and low excitability threshold. The first excitator exhibits nearly periodic firings with the firing number σ_{12} close to 0.8 while the second one performs periodic firings with $n^e_3 = 1$ and $n^o_2 = 2$ (i.e., with the firing number $\sigma_{32} = 0.5$). The excitation diagrams in Figure 8 document the existence of unsynchronized firings in the linear **EOE** array especially within the region of fractional firings which covers significant part of the phase excitation diagram

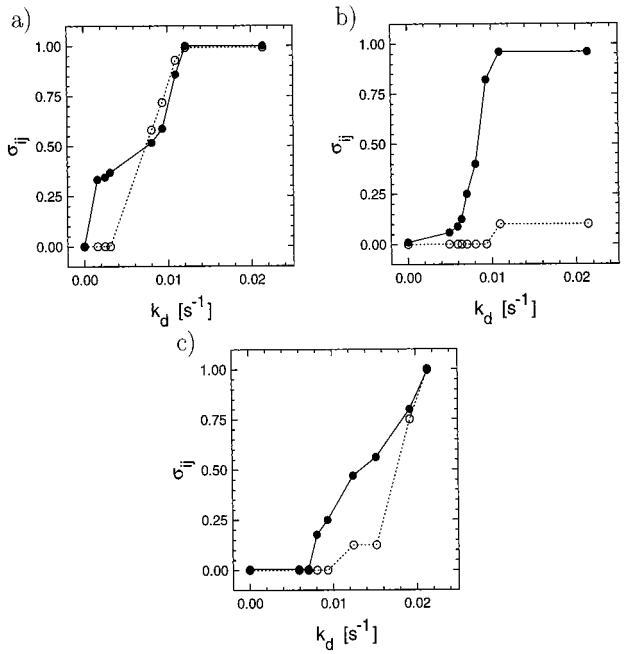

Figure 8. Experimental excitation diagrams for linear three-array **EOE**. (●) firing number σ_{12}. (○) Firing number σ_{32}. Inlet KBr concentration: (a) $Y^0_1 = Y^0_3 = 0.003$ mol dm^{-3}, (b) $Y^0_1 = Y^0_3 = 0.004$ mol dm^{-3}, (c) $Y^0_1 = Y^0_3 = 0.005$ mol dm^{-3}.

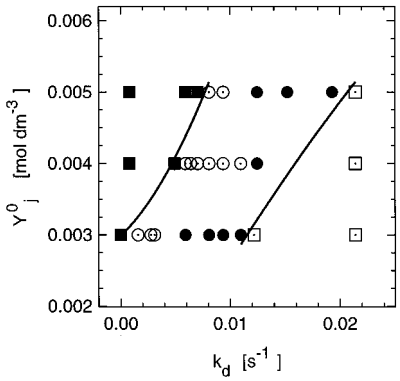

Figure 9. Experimental phase excitation diagram for linear three-array **EOE**, ($j \equiv 1, 3$). (■) $\sigma_{12} = \sigma_{32} = 0$. (⊙) $0 < (\sigma_{12}, \sigma_{32}) < 1/2$. (●) $1/2 < (\sigma_{12}, \sigma_{32}) < 1$. (⊡) $\sigma_{12} = \sigma_{32} = 1$.

(see Figure 9). Similar to the **OEE** array no substantial continuous subregions with constant values of firing numbers can be found in the regions of the fractional firings in excitation diagrams of the **EOE** array (cf Figure 8). The differences of experimentally determined firing numbers in both excitators are probably due to subtle sensitivity of the oscillatory−excitatory regimes to differences of the coupling strengths among the individual excitators and the oscillator, which are unavoidable in experiments. Precise adjustment of all excitator−oscillator coupling strengths to the same value seems to be the ultimate condition for obtaining synchronized firings in arrays with several excitators directly coupled to the same oscillator.

*Circular Three-Array **cOEE***. Direct mutual coupling among the excitatory cells in this circular array stimulates synchronized firings of both excitators (cf Figures 5c and 10) because the mutual coupling of both excitators compensates for experimental inaccuracy of the setting of the coupling strengths of both excitators to the oscillator. Only very small differences of firing numbers σ_{21} and σ_{31} arising due to experimental errors can be observed in the excitation diagrams in Figure 10 at all values of the inlet KBr concentration. Mutual transfer of the excitatory

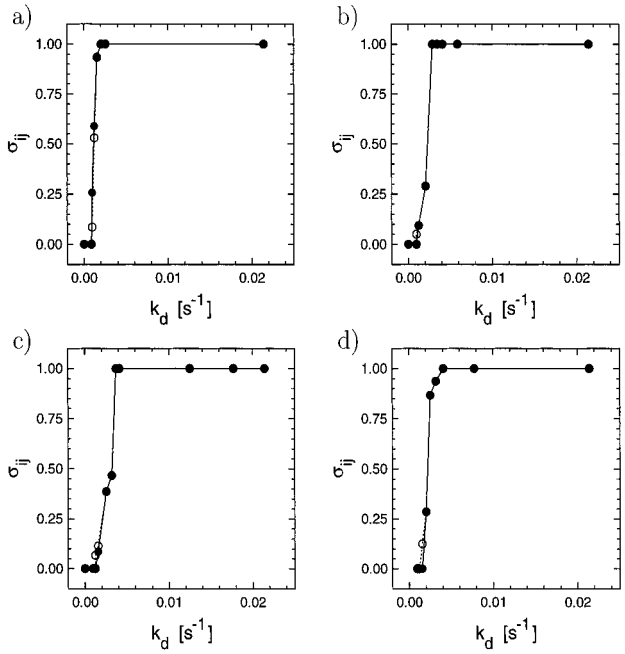

Figure 10. Experimental excitation diagrams for circular three-array **cOEE**. (●) Firing number σ_{21}. (○) Firing number σ_{31}. Inlet KBr concentration: (a) $Y_2^0 = Y_3^0 = 0.003$ mol dm^{-3}, (b) $Y_2^0 = Y_3^0 = 0.004$ mol dm^{-3}, (c) $Y_2^0 = Y_3^0 = 0.005$ mol dm^{-3}, (d) $Y_2^0 = Y_3^0 = 0.006$ mol dm^{-3}.

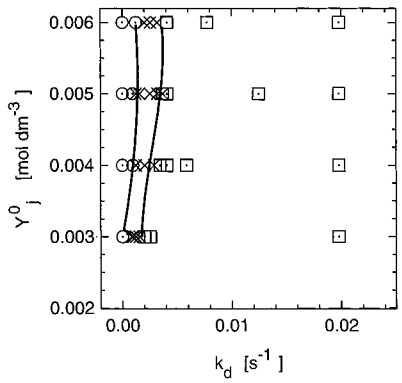

Figure 11. Experimental phase excitation diagram for circular three-array **cOEE**, ($j \equiv 2, 3$). (⊙) $\sigma_{21} = \sigma_{31} = 0$. (×) $0 < (\sigma_{21}, \sigma_{31}) < 1$. (⊡) $\sigma_{21} = \sigma_{31} = 1$.

response among the directly coupled excitators minimizes the threshold value of the coupling strength coefficient necessary for firings to occur (cf Figures 8 and 9 for the threshold values in the linear **EOE** array with decoupled excitators). The transition from no excitations to full excitations is very steep and the region of fractional excitation regimes in the phase excitation diagram in Figure 11 is therefore very narrow. The value of the inlet KBr concentration (threshold of the excitability) has only marginal effect on the width and position of this region. Again no subregions with constant values of firing numbers are detectable in the region of fractional excitations. The regime of full excitation occupies most of the experimentally accessible parametric plane in Figure 11.

The experimental results described in previous paragraphs allow for formulation of several generally valid conclusions on the observed oscillatory−excitatory patterns: Certain minimum (nonzero) coupling strength among the oscillator and the coupled excitator is required for the excitation to arise in the excitatory cell(s). The threshold value of the coupling strength depends both on the value of the threshold of the excitability and the

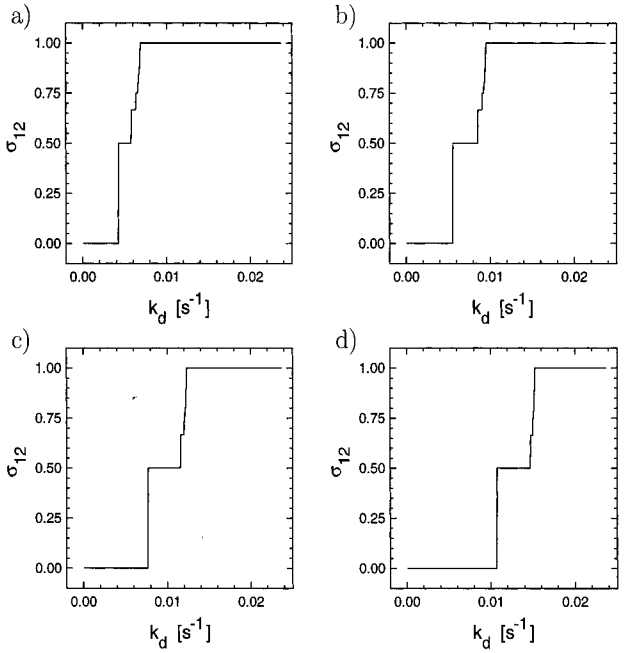

Figure 12. Simulated excitation diagrams for two-array **OE**. Inlet KBr concentration: (a) $Y_2^0 = 0.003$ mol dm^{-3}, (b) $Y_2^0 = 0.004$ mol dm^{-3}, (c) $Y_2^0 = 0.005$ mol dm^{-3}, (d) $Y_2^0 = 0.006$ mol dm^{-3}.

configuration of the cell array. The values of firing numbers in the regions of fractional excitation regimes are highly sensitive to the strength of the coupling among the excitator and the oscillator. The rise of the firing number value from 0 (no excitations) to 1 (full excitations) happens usually within quite narrow interval of the coupling strength. Highly precise adjustments of the coupling strength coefficient are therefore required in order to obtain the oscillatory−excitatory pattern with the required particular value of the firing number. The differences of coupling strengths due to experimental inaccuracy in arrays with two or more excitators and one oscillator result in the failure of excitations or desynchronization of firings. The synchronization of the firings can be achieved by introducing direct mutual coupling of the adjacent excitators in the array. The threshold value of the coupling strength is significantly lowered in arrays with direct excitator−excitator coupling.

4.2. Simulated Oscillatory−Excitatory Patterns. The oscillatory−excitatory patterns in the same array configurations as those used in experiments were studied by numerical simulations based on the mathematical model described in the section 3 and in the Appendix. The excitation diagrams are used for classification and analysis of the simulated oscillatory−excitatory patterns.

*Two-Array **OE***. The excitation diagrams in Figure 12 agree, in principle, with experimental results. There are, however, noticeable differencies of the threshold values of the coupling strength, their increase with the increasing inlet KBr concentration, and the position and width of regions of particular dynamical regimes in Figures 12 and 3. The presence of substantial plateaus of the excitation regimes with $\sigma_{21} = {}^1/_2$ and $\sigma_{21} = {}^2/_3$ in all simulated excitation diagrams is the most apparent difference among the results of the experiments and numerical simulations. The fractional excitation regimes with other values of firing numbers occur only within very narrow intervals of the coupling strength coeffient. Almost no excitatory regimes with $\sigma_{21} < {}^1/_2$ were detected in simulations despite very fine resolution used in the construction of Figure 12 (and also of all diagrams discussed further). Most dynamical

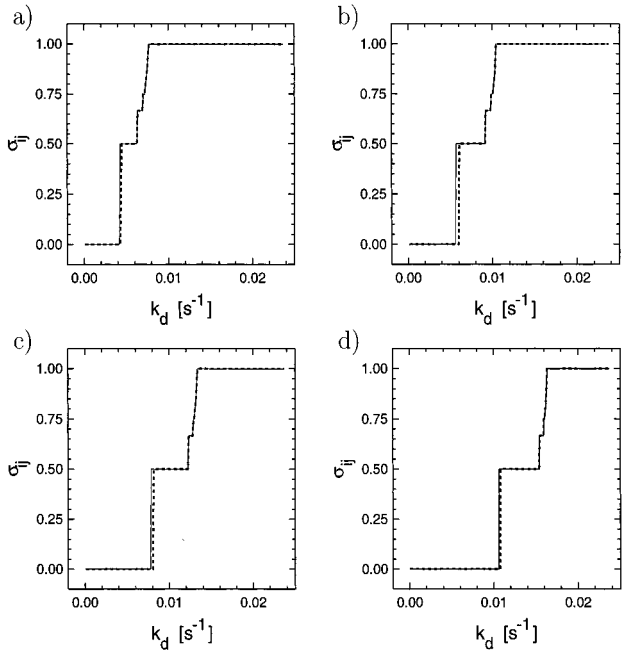

Figure 13. Simulated excitation diagrams for linear three-array **OEE**. (—) firing number σ_{21}. (– –) firing number σ_{31}. Inlet KBr concentration: (a) $Y_2^0 = Y_3^0 = 0.003$ mol dm^{-3}, (b) $Y_2^0 = Y_3^0 = 0.004$ mol dm^{-3}, (c) $Y_2^0 = Y_3^0 = 0.005$ mol dm^{-3}, (d) $Y_2^0 = Y_3^0 = 0.006$ mol dm^{-3}.

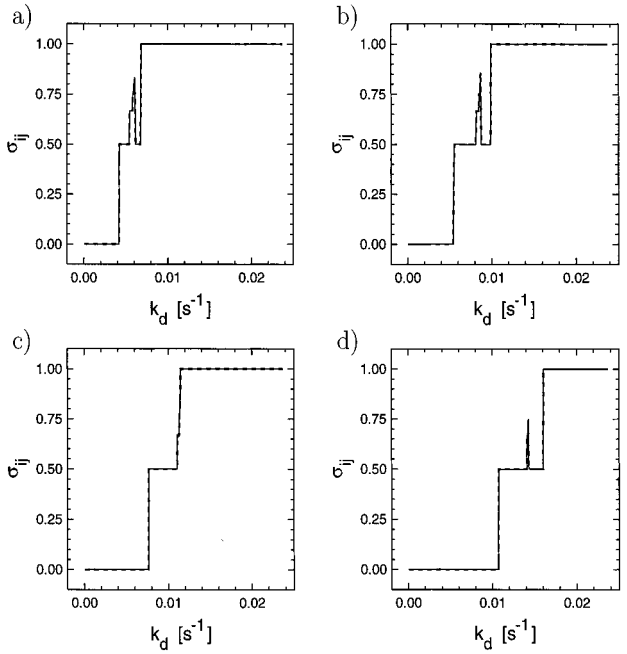

Figure 14. Simulated excitation diagrams for linear three-array **EOE**. (—) firing number σ_{12}. (– –) firing number σ_{32}. Inlet KBr concentration: (a) $Y_1^0 = Y_3^0 = 0.003$ mol dm^{-3}, (b) $Y_1^0 = Y_3^0 = 0.004$ mol dm^{-3}, (c) $Y_1^0 = Y_3^0 = 0.005$ mol dm^{-3}, (d) $Y_1^0 = Y_3^0 = 0.006$ mol dm^{-3}.

patterns corresponding to excitation diagrams in Figure 12 are periodic (period-1, period-2, and period-3); the aperiodic regimes were detected only at the values of firing number very close to 1. The noisy character of the coupling among the reaction cells (cf section 4.3) and the experimental error in controlling the coupling strengths are possible reasons of missing plateaus with constant values of firing numbers in the experimental excitation diagrams and of other differencies among the experimental and numerical results.

*Linear Three-Array **OEE***. The simulated excitation diagrams in Figure 13 resemble the structure of simulated excitation diagrams for the **OE** array. The threshold values of the coupling strengths are practicaly the same and noticeable differences of the diagrams are observable only in the region of higher values of firing numbers. The only oscillatory−excitatory regimes occupying substantial subintervals of the coupling strength values are again periodic regimes with the firing numbers $\sigma_{21} = \sigma_{31} = {}^1/_2$ and $\sigma_{21} = \sigma_{31} = {}^2/_3$. The regimes with $\sigma_{ij} > {}^2/_3$ persist only over very narrow intervals of the coupling strength. The firings in both excitatory cells in the linear **OEE** array are mostly synchronized. The possible unsynchronized excitations can be deduced from Figure 13; however, they exist in a very narrow interval of the coupling strength values located between the no-excitation regime and the excitation regimes with $\sigma_{ij} = {}^1/_2$. No complete extinction of excitations in the second excitatory cell (observed in experiments, cf. Figure 6b) was found in simulations. The inequality of both coupling strengths in the experiments is probable reason of this observation.

*Linear Triple Array **EOE***. Numerical simulations of oscillatory−excitatory patterns in this coupled cell array predicts only synchronized firings of both excitators (cf Figure 14). The threshold value of coupling strength increases with the increasing inlet KBr concentration and the most substantial fractional excitation regimes are characterized by firing numbers ${}^1/_2$ and ${}^2/_3$. The subregions of excitation regimes with $\sigma_{ij} = {}^2/_3$ are either embedded within the region occupied by regimes with the firing number $\sigma_{ij} = {}^1/_2$ or located between this region and the region of full excitation. The detailed numerical analysis showed subtle and complicated structure of excitation regimes in the parametric space. The periodic excitations with $\sigma_{ij} = {}^1/_2$ alternate with both periodic and aperiodic excitations with ${}^1/_2 < \sigma_{ij} < {}^4/_5$ in dependence on the inlet KBr concentration. The size of the sub-regions with particular firing numbers is very small and these regimes would be therefore hardly detectable in experiments.

*Circular Three-Array **cOEE***. Only synchronized excitations in both excitatory cells ($\sigma_{21} = \sigma_{31}$) are predicted by numerical simulations of the **cOEE** array (cf Figure 15). This fact agrees with experimental observations (cf Figure 10). The threshold values of the coupling strength necessary for excitations to arise in **E** cells are significantly lowered in experimental excitation diagrams compared to simulated ones. The threshold values of k_d obtained by simulations, however, correspond to threshold values in other simulated arrays (cf Figures 12−14). The simulated excitation diagrams for the **cOEE** array predict the existence of the excitation regimes with firing numbers $\sigma_{ij} = {}^1/_2$ over relatively wide intervals of the coupling strength coefficient k_d. The regions of these excitation regimes were not detected in experiments. The differences of dynamical behavior of the **cOEE** array predicted by simulations and observed in experiments are probably connected with net liquid circulation through the array due to pumping effects of the impellers (in linear cell arrays the net circulation does not exist because of the closed intercell barriers). The noisy character of cell−cell coupling can be an additional factor responsible for smaller extent of excitation regimes with $\sigma_{ij} = {}^1/_2$ in the experimental excitation diagrams (cf section 4.3).

The oscillatory−excitatory patterns predicted by numerical simulations for studied cell arrays share some common features. The most part of the phase excitation diagram area (i.e. of the parametric plane "coupling strength" vs "inlet KBr concentration") is in most cases covered either by no-excitation pattern or the full excitation pattern region. The transition among these two patterns is steep with only low number of fractional excitation regimes. Almost no dynamical patterns with the firing

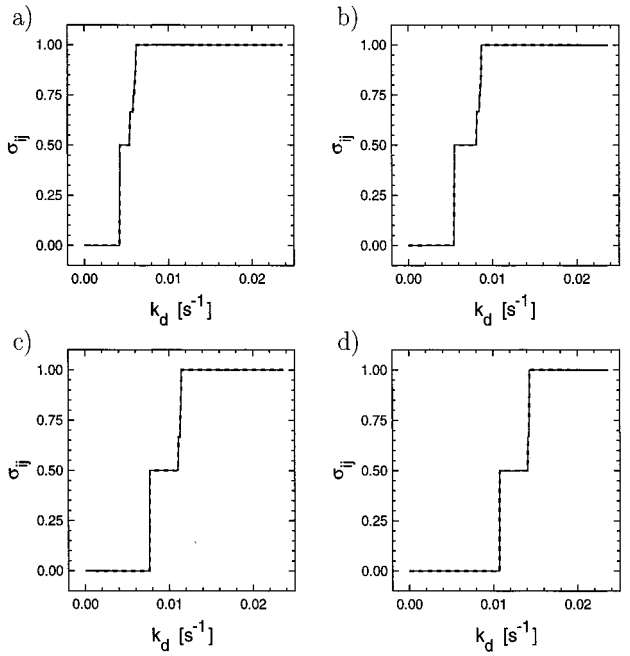

Figure 15. Simulated excitation diagrams for circular three-array **cOEE**. (—) firing number σ_{21}. (— —) Firing number σ_{31}. Inlet KBr concentration: (a) $Y_2^0 = Y_3^0 = 0.003$ mol dm^{-3}, (b) $Y_2^0 = Y_3^0 = 0.004$ mol dm^{-3}, (c) $Y_2^0 = Y_3^0 = 0.005$ mol dm^{-3}, (d) $Y_2^0 = Y_3^0 = 0.006$ mol dm^{-3}.

numbers lower than 0.5 were detected. The structure of the excitation diagrams for all studied arrays do not differ significantly.

The three categories of coupled cell two- and three-arrays differing in the observed oscillatory−excitatory dynamical patterns can be established on the basis of numerical simulations: (i) the arrays with one oscillator connected to single excitator (the arrays **OE**, **OEE**, and **OOE**), (ii) the arrays with two oscillators connected to the same excitator (the arrays **OEO** and **cOOE**), and (iii) the arrays with two excitators coupled to the same oscillator (the arrays **EOE** and **cOEE**). The excitation and phase excitation diagrams of the individual arrays of the first category exhibit high similarity and generally quite high threshold values of the coupling strength. The threshold values of the coupling strength are remarkably reduced (approximately to one-half of the value in the category (i)) in the arrays of the second category where two oscillators synchronously perturb the same oscillator. The threshold values of the coupling strength in the arrays of the third category where the single oscillator perturbs simultaneously two excitators are again remarkably high (comparable to values in the arrays of the first category). The point of onset of excitations and also the position of the regions with particular excitation regimes can be easily manipulated by changing the number of the oscillators (excitators) coupled to the same excitator (oscillator).

The numerically simulated excitation and phase excitation diagrams generally agree well with the diagrams constructed from experimental data. The onset of firings and the sizes of regions of individual excitatory patterns in certain diagrams, however, differ remarkably. The experimental errors in setting the coupling strengths in the array, the noisy character of the coupling (see next paragraph) and the difference of time scales of the BZ reaction and of the used kinetic model can explain the observed differencies. Noise is inherently present in all real chemical and biological systems. Different noise levels can generally cause differences in the initiation of excitation in the threshold systems and also in the extent of propagation of the

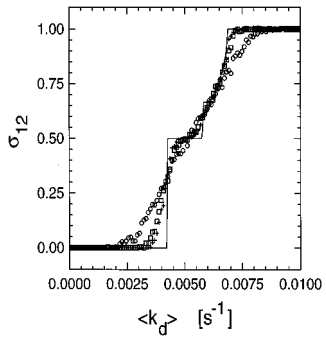

Figure 16. Effect of the noise level on numerically simulated excitation diagrams for the **OE** two-array. $<k_d>$ denotes mean value of the coupling strength coefficient. (—) noise level 0%. (+) noise level 0.1%. (□) noise level 0.2%. (○) noise level 0.5%. Inlet KBr concentration: 0.003 mol dm^{-3}.

evoked excitations. In the following we shall discuss the effects of low level noise on the simulated oscillatory−excitatory patterns.

4.3. Effects of Noisy Coupling. The possible effects of noisy coupling on synchronizations of three coupled BZ oscillators have been reported recently (see Nevoral et al.[42]). Here we study the effects of the noisy coupling in the oscillatory−excitatory cell arrays in order to explain some of the differences among the experimentally observed and numerically simulated oscillatory−excitatory patterns. The coupling strength coefficient k_d was considered to be a correlated gamma-distributed stochastic process generated by a stochastic differential equation solved[46] simultaneously with the balance eqs 1 (see Nevoral et al.[42] for details). Other kinds of the noise imposed to the coupling strength could be also considered resulting in different dynamical regimes in the simulated oscillatory excitatory arrays. The gamma-distributed noise, however, corresponds to actual coupling strength fluctuations which can gain only nonnegative values (contrary, for example, to the commonly used Gaussian noise). The short-time correlation of the fluctuations considered in simulations relates to correlation of hydrodynamical fluctuations in the intercell channels due to the forces of inertia.

The effects of the level of the noise imposed on the coupling strength on the value of firing number in the **OE** two-array are shown in Figure 16. The level of noise is expressed by means of the variance-to-mean ratio. Already very low noise level (0.05%) causes high number of the fractional excitation regimes (not observed in simulations without noise) to appear in the excitation diagram. The higher the level of the noise the more the excitation diagrams become smeared, (i.e., no substantial plateaus with constant firing number exist). The threshold value of the mean value of the coupling strength shifts toward lower values and the width of the fractional excitations region increases with the increasing noise level. The noisy coupling (due, for example, to turbulent hydrodynamical fluctuations) can therefore explain the high number of the fractional excitation regimes detected in experiments and not predicted by numerical simulations. The comparison of the experimental excitation diagrams with the numerically simulated ones (both with and without noise) is shown in Figure 17. The agreement of experimental data with the excitation diagram simulated with the noisy coupling is, generally, very good. The most obvious deviations are observable in Figure 17a (i.e., at the lowest value of the threshold of the excitability of the BZ reaction). Here the most probable reason of these deviations is high relative imprecision of setting of the coupling strength value in the experiments. This conclusion is supported also by results in Figures 17b−d, where the deviations among experi-

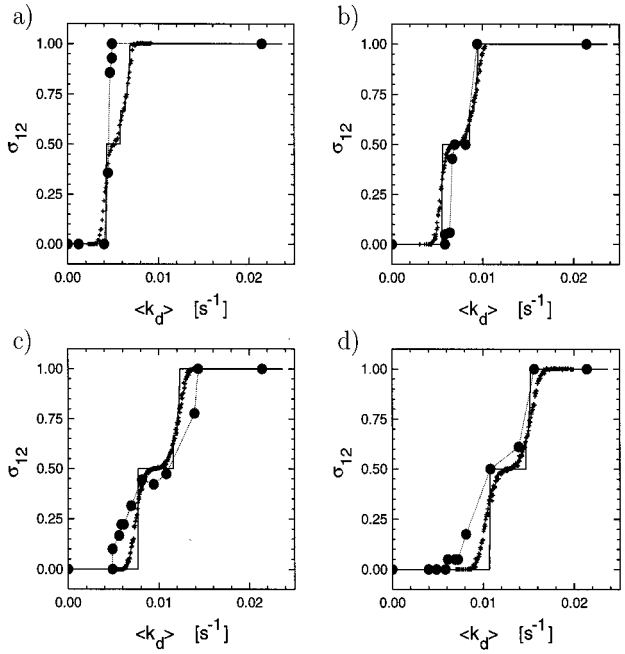

Figure 17. Simulated and experimental excitation diagrams for two-array **OE**. $< k_d >$ denotes mean value of the coupling strength coefficient. (—) noise level 0%. (+) noise level 0.1%. (●) experimental data. Inlet KBr concentration: (a) $Y^0_2 = 0.003$ mol dm^{-3}. (b) $Y^0_2 = 0.004$ mol dm^{-3}, (c) $Y^0_2 = 0.005$ mol dm^{-3}, (d) $Y^0_2 = 0.006$ mol dm^{-3}.

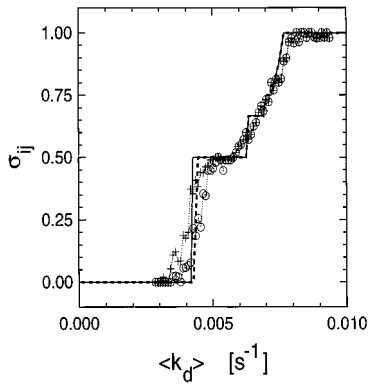

Figure 18. Effect of noisy coupling on excitations in the linear OEE array ($j \equiv 2, 3$). $<k_d>$ denotes mean value of the coupling strength coefficient. (—) Firing number σ_{21}, noise level 0%. (— —) Firing number σ_{31}, noise level 0%. (+) Firing number σ_{21}, noise level 0.1%. (○) Firing number σ_{31}, noise level 0.1%. Inlet KBr concentration: 0.003 mol dm^{-3}.

mental and simulated data are most obvious at low coupling strength values close to the threshold value. Figure 18 depicts the effects of the noisy coupling on the oscillatory−excitatory patterns in the linear **OEE** array. The excitation diagrams from both cells are again deeply blurred by the noise applied to the coupling strength compared to the diagram with the coupling without noise. The noisy coupling leads, moreover, also to remarkable desynchronization of firings in both excitators in regimes of fractional excitations with $\sigma_{ij} < {}^1/_2$. The noisy coupling among the cells can, therefore, account for the desynchronizations of firings observed in experiments (cf Figure 6).

The noisy coupling among the cells is not the only possible explanation of the discrepancies among the experimental results and the oscillatory−excitatory regimes predicted by numerical simulations. The time delay in the cell−cell communication due to nonzero residence time of the liquid in the channels connecting the cells in the experimental setup (especially at low values of the coupling strength) can also strongly influence dynamical patterns in the systems of coupled oscillators and excitators where the precise timing of oscillatory and excitatory events is of the ultimate importance. The chemical reactions taking place inside the connecting channels can, moreover, be a cause of the nonlinear character of the cell−cell coupling contributing also to the difference among the experimental and simulated results.

5. Conclusions

Experimental and numerical studies of the propagation of excitations in two- and three-arrays of mass exchange coupled CSTRs with the BZ reaction have clearly demonstrated that resonance regimes observed in the cell array and successful or failing propagation of excitation within the network depend both on the level of threshold and the intensity of mutual mass coupling among the cells and vary for different configurations of excitable and oscillatory units in the array. Certain minimum coupling strength intensity is necessary in order to attain firings in excitable cells. The threshold value significantly increases when the threshold of the excitability of the BZ reaction is increasing. Comparison of behavior of cell arrays containing different numbers of oscillators and excitators has shown that threshold values of the coupling strength for the propagation of excitations are nearly halved if the array contains two oscillators and increase if two excitators are coupled with a single oscillator and they are also significantly affected by linear or circular configuration of the array. The experimental results clearly demonstrated how the spatiotemporal firing patterns in a cell array can be controlled by proper setting of the threshold value (by means of the inlet KBr concentration), by setting of the coupling strengths and by geometrical configuration of the array. The results from the two- and three-membered arrays presented in this paper can be extended to arrays with more units if one considers the larger arrays to be composed of the above basic two- and three-membered elements. Some of the firing patterns observed in experiments, namely in the circular three-array with two excitators, exhibit strong absence of the partial excitation regimes and significant decrease of the threshold level of the coupling strength. The circular arrays with several excitators therefore minimize the magnitude of the stimulation required for maintaining the excitators in the fully excited state.

The simulated dynamical oscillatory−excitatory regimes in arrays with two excitators exhibit pronounced tendency to synchronized firings. In arrays with two oscillators and a single excitator the firing numbers with respect to both oscillators do not differ. The observed regimes, however, possesed only the in-phase modes (i.e., the oscillators were perfectly synchronized). More complex oscillatory−excitatory regimes with the phase transitions and synchronization of oscillators can be expected in arrays with phase-shifted oscillators.

The oscillatory−excitatory patterns observed in the experiments agree qualitatively well with the results of modeling. Certain differencies, however, are observable. The transition from the no-excitation regime to the full excitation regime is usually more steep in simulated diagrams than in the experimental ones. The only exception is circular array with two excitators (**cOEE**) where the direct coupling of both excitators yielded steeper transition in experiments. The presence of extended plateaus with firing number equal to ${}^1/_2$ in excitation diagrams is the characteristic feature of the simulated data. The noise is, however, always imposed to the coupling strength among the cells in experiments and a high number of the fractional excitation regimes arise as a consequence of the noisy

coupling. This experimental observation was verified by numerical simulations. Some of the array configurations, however, tend to be significantly robust with respect to the noisy coupling (e.g., the circular (**cOEE**) array). An intrinsic interconnection of the excitable units in oscillatory−excitatory arrays with higher number of single units therefore represents a possible way how to make the resulting structure more stable and robust from the point of view of the errorless information processing.

The desynchronization of the firings in linear arrays with two excitators was frequently encountered in experiments and can be explained by noisy character of the cell−cell coupling. Comparison of simulations based on the three-component model of the BZ reaction with experimental results has shown that satisfactory semiquantitative agreement can be obtained if low level noise in the intensity of mutual mass coupling among the cells is considered. The noisy coupling vastly increases the values of the detected firing number.

The structure of simulated phase excitation diagrams for all investigated arrays is relatively simple. Weak resonances with the firing number values lower than $^1/_2$ were seldom detected. The only oscillatory−excitatory regimes with the extended regions of existence within parametric space are regimes with firing numbers equal to 0, $^1/_2$, $^2/_3$, $^3/_4$, and 1, respectively. Other dynamical regimes with firing numbers greater than $^1/_2$ are very hard to detect and require extremely precise adjustment of control parameters. Phase excitation diagrams for linear three-array of coupled excitators constructed by Nevoral et al.[42] both from experimental and simulated data exhibit much more complex structure. In their experiments and simulations, however, both the amplitude and the period of periodic pulsed perturbations were adjustable control parameters contrary to the above studied oscillatory−excitatory arrays where the amplitude and the period of the oscillatory pacemakers were fixed.

Further generalization of the above results based on the modeling studies with other oscillator−excitator systems will be the subject of the following studies. Basic control parameters available for affecting dynamics of the oscillatory−excitatory arrays are coupling strengths, excitability threshold and internal configuration of an array (linear or circular, etc.). The effects of the levels of noise will be also considered. Generic conclusions could help in the interpretation of experimental observations on small neural networks in biological systems.

Acknowledgment. The authors thank the Grant Agency of the Czech Republic (Grant 203/96/1507) and the Ministry of Education of the Czech Republic (Grant VS96073) for support of this project.

6. Appendix

The dimensionless concentrations of the reaction components of the three-variable model of the BZ reaction are defined by the relations (see Ševčíková et al.[44] for details on the BZ reaction kinetics and the model itself)

$$x_j \equiv \frac{2k_4}{k_5HA}X_j \tag{A1}$$

$$y_j \equiv \frac{k_2}{k_5A}Y_j \tag{A2}$$

$$z_j \equiv \frac{2k_4k_7B}{(k_5HA)^2}Z_j \tag{A3}$$

TABLE 1: Rate Constants at 28 °C and Other Model Parameters

parameter	value	unit(s)
k_2	2.499×10^6	$dm^6\ mol^{-2}\ s^{-1}$
k_3	4.508	$dm^9\ mol^{-3}\ s^{-1}$
k_4	3709.9	$dm^3\ mol^{-1}\ s^{-1}$
k_5	105.23	$dm^6\ mol^{-2}\ s^{-1}$
k_{-5}	6.324×10^7	$dm^3\ mol^{-1}\ s^{-1}$
k_6	2.258×10^5	$dm^6\ mol^{-2}\ s^{-1}$
k_{-6}	1.158×10^4	$dm^3\ mol^{-1}\ s^{-1}$
k_7	0.948	$dm^3\ mol^{-1}\ s^{-1}$
k_9	2.056×10^{-6}	s^{-1}
q	0.8	
A	0.100	mol dm^{-3}
B	0.200	mol dm^{-3}
$C \equiv Z_j^0$	0.006	mol dm^{-3}
H	0.5293	mol dm^{-3}
X_j^0	0.0	mol dm^{-3}
Y_j^0	adjustable	mol dm^{-3}
k_0	5.556×10^{-4}	s^{-1}
k_d	adjustable	s^{-1}

where X_j, Y_j, and Z_j are the molar concentrations of respective components. Dimensionless time τ is defined as

$$\tau \equiv k_7Bt \tag{A4}$$

Dimensionless model parameters in eqs 1−4 are defined by the relations

$$\epsilon \equiv \frac{k_7B}{k_5HA} \tag{A5}$$

$$p \equiv \frac{2k_3k_4}{k_2k_5} \tag{A6}$$

$$\sigma \equiv \frac{2k_4}{k_2H} \tag{A7}$$

$$\kappa_{-5} \equiv \frac{2k_4\epsilon^2}{(k_6H)}2k_{-5} \tag{A8}$$

$$\kappa_{-6} \equiv \frac{1}{2k_4\epsilon}k_{-6} \tag{A9}$$

$$\kappa_9 \equiv \frac{2k_4B}{(k_5HA)^2}k_9 \tag{A10}$$

The reciprocal value of the dimensionless residence time κ_0 and the dimensionless coupling strength coefficient κ_d are defined as follows

$$\kappa_0 \equiv \frac{k_0}{k_7B} \tag{A11}$$

$$\kappa_d \equiv \frac{k_d}{k_7B} \tag{A12}$$

The symbols k_l, (l = 2, 3, 4, 5, 6, 7, 9, −5, and −6) in the above equations denote kinetic constants of the Oregonator based model of the BZ reaction mechanisms (see Mori et al.[43] and Ševčíková et al.[44]); k_0 is the reciprocal value of the residence time in a single cell. *A*, *B*, *C*, and *H* are inlet concentrations of malonic acid, $NaBrO_3$, Ce^{4+}, and H^+, respectively. Symbol $u_j \equiv \xi_{4j}$ in eqs 2 and 4 denotes dimensionless concentration of

reaction intermediate $HBrO_2^+$ which is considered to be in a pseudo-stationary state

$$u_j \equiv u_j(x_j,z_j) = \frac{2x_j(2 + \kappa_{-6}z_j)}{(c - z_j) + \sqrt{(c - z_j)^2 + 8\kappa_{-5}x_j(2 + \kappa_{-6}z_j)}} \tag{A13}$$

where the constant c is defined as

$$c \equiv \frac{2k_4k_7\mathrm{B}}{(k_5HA)^2}C \tag{A14}$$

The values of dimensional rate constants and other parameters used in the definitions A1−A14 are given in Table 1.

References and Notes

(1) Marek, M.; Stuchl, I. *Biophys. Chem.* **1975**, *3*, 241.
(2) Nakajima, K.; Sawada, Y. J. *J. Chem. Phys.* **1980**, *72*, 2231.
(3) Bar-Eli, K.; Reuveni, S. J. *J. Phys. Chem.* **1985**, *89*, 1329.
(4) Bar-Eli, K. *J. Phys. Chem.* **1984**, *88*, 3616.
(5) Boukalouch, M.; Elezgaray, J.; Arneodo, A.; Boissonade, J.; De Kepper, P. *J. Phys. Chem.* **1987**, *91*, 5843.
(6) Crowley, M. F.; Epstein, I. R. *J. Phys. Chem.* **1989**, *93*, 2496.
(7) Stuchl, I.; Marek, M. *J. Chem. Phys.* **1982**, *77*, 1607.
(8) Yoshikawa, K.; Fukunaga, K.; Kawakami, H. *Chem. Phys. Lett.* **1990**, *174*, 273.
(9) Laplante, J.-P.; Erneux, T. *J. Phys. Chem.* **1992**, *98*, 6537.
(10) Booth, V.; Erneux, T.; Laplante, J.-P. *J. Phys. Chem.* **1994**, *98*, 6537.
(11) Doumbouya, S. I.; Schneider, F. W. *J. Phys. Chem.* **1993**, *97*, 6945.
(12) Doumbouya, S. I.; Münster, A. F.; Doona, C. J.; Schneider, F. W. *J. Phys. Chem.* **1993**, *97*, 1025.
(13) Hauser, M. J. B.; Schneider, F. W. *J. Chem. Phys.* **1994**, *100*, 1058.
(14) Weiner, J.; Schneider, F. W.; Bar-Eli, K. *J. Phys. Chem.* **1989**, *93*, 2704.
(15) Chevalier, T.; Freund, A.; Ross, J. *J. Chem. Phys.* **1991**, *95*, 308.
(16) Roesky, P. W.; Doumbouya, S. I.; Schneider F. W. *J. Phys. Chem.* **1993**, *97*, 398.
(17) Weiner, J.; Holz, R.; Schneider, F. W.; Bar-Eli, K. *J. Phys. Chem.* **1992**, *96*, 8915.
(18) Holz, R.; Schneider, F. W. *J. Phys. Chem.* **1993**, *97*, 12239.
(19) Yoshimoto, M.; Yoshikawa, K.; Mori, Y. *Phys. Rev.* E **1993**, *47*, 864.
(20) Hjelmfelt, A.; Schneider, F. W.; Ross, J. *Science* **1993**, *260*, 335.
(21) Hjelmfelt, A.; Weinberger, E. D.; Ross, J. *Proc. Natl. Acad. Sci. U.S.A.* **1991**, *88*, 10983.
(22) Hjelmfelt, A.; Weinberger, E. D.; Ross, J. *Proc. Natl. Acad. Sci. U.S.A.* **1992**, *89*, 383.
(23) Hjelmfelt, A.; Ross, J. *Proc. Natl. Acad. Sci. U.S.A.* **1992**, *89*, 388.
(24) Hjelmfelt, A.; Ross, J. *J. Chem. Phys.* **1993**, *97*, 7988.
(25) Hjelmfelt, A.; Ross, J. *Proc. Natl. Acad. Sci. U.S.A.* **1994**, *91*, 63.
(26) Laplante, J.-P.; Pemberton, M.; Hjelmfelt, A.; Ross, J. *J. Phys. Chem.* **1995**, *99*, 10063.
(27) Botré, C.; Lucarini, C.; Memoli, A.; D′Ascenzo, E. *Bioelectrochem. Bioenerg.* **1981**, *8*, 201.
(28) Crowley, M. F.; Field, R. J. *J. Phys. Chem.* **1986**, *90*, 1907.
(29) Schneider, F. W.; Hauser, M. J. B.; Reising, J. *Ber. Bunsen-Ges. Phys. Chem.* **1993**, *97*, 55.
(30) Zeyer, K.-P.; Münster, A. F.; Hauser, M. J. B.; Schneider, F. W. *J. Chem. Phys.* **1994**, *101*, 5126.
(31) Marek, M.; Schreiber, I. Chaos in Forced and Coupled Oscillators and Excitators. In *Chaos in Chemistry and Biochemistry*; Field, R. J.; Györgyi, L., Eds.; World Scientific: Singapore; 1993; p 87.
(32) Dolník, M.; Finkeová, J.; Schreiber, I.; Marek, M. *J. Phys. Chem.* **1989**, *93*, 2764.
(33) Finkeová, J.; Dolník, M.; Hrudka, B.; Marek, M. *J. Phys. Chem.* **1990**, *94*, 4100.
(34) Kosek, J.; Schreiber, I.; Marek, M. *Philos. Trans. R. Soc. London, Ser. A* **1994**, *347*, 643.
(35) Dolník, M.; Marek, M. *J. Phys. Chem.* **1991**, *95*, 7262.
(36) Dolník, M.; Marek, M.; Epstein, I. R. *J. Phys. Chem.* **1992**, *96*, 3218.
(37) Dolník, M.; Kosek, J.; Votrubová, V.; Marek, M. *J. Phys. Chem.* **1994**, *98*, 3707.
(38) Terman, D.; Lee, E. *SIAM J. Appl. Math.* **1997**, *57*, 252.
(39) Kopell, N.; Somers, D. C. *J. Math. Biol.* **1995**, *33*, 261.
(40) Stössel, R.; Münster, A. F. *Chem. Phys. Lett.* **1996**, *263*, 789.
(41) Marek, M.; Svobodová, E. *Biophys. Chem.* **1975**, *3*, 263.
(42) Nevoral, V.; Votrubová, V.; Hasal, P.; Schreiberová, L.; Marek, M. *J. Phys. Chem. A* **1997**, *101*, 4954.
(43) Mori, E.; Schreiber, I.; Ross, J. *J. Phys. Chem.* **1991**, *95*, 9359.
(44) Ševčíková, H.; Schreiber, I.; Marek, M. *J. Phys. Chem.* **1996**, *100*, 19153.
(45) Kosek, J.; Marek, M. *J. Phys. Chem.* **1993**, *97*, 120.
(46) Kloeden, P. E.; Platen, E. *Numerical Solution of Stochastic Differential Equations*; Springer: Berlin, 1995.